Acta Materialia 98 (2015) 367–376

Contents lists available at ScienceDirect

Acta Materialia

journal homepage: www.elsevier.com/locate/actamat

Ab initio study of compositional trends in solid solution strengthening in metals with low Peierls stresses

Duancheng Ma [a,*], Martin Friák [a,b], Johann von Pezold [a], Jörg Neugebauer [a], Dierk Raabe [a]

[a] Max-Planck-Institut für Eisenforschung GmbH, Max-Planck-Straße 1, 40237 Düsseldorf, Germany
[b] Institute of Physics of Materials, Academy of Sciences of the Czech Republic, v.v.i, Žižkova 22, Brno, Czech Republic

ARTICLE INFO

Article history:
Received 15 March 2015
Accepted 20 July 2015

Keywords:
Solid solution strengthening
DFT
Ab-initio
Al alloys
Mg alloys
Ni alloys
Mg basal slip

ABSTRACT

We identify and analyze general trends governing solid solution strengthening in binary alloys containing solutes across the Periodic table using quantum-mechanical calculations. Here we present calculations for the model system of Al binary solid solutions. The identified trends originate from an approximately parabolic dependence of two strengthening parameters to quantitatively predict the solid solution strengthening effect, i.e. the volume and slip misfit parameters. The volume misfit parameter shows a minimum (concave-up behavior) as a function of the solute element group number in the periodic table, whereas the slip misfit parameter shows a maximum (concave-down behavior). By analyzing reported data, a similar trend is also found in Ni and Mg (basal slip) binary systems. Hence, these two strengthening parameters are strongly anti-correlated, which can be understood in terms of the Fermi level shift in the framework of free electron model. The chemical trends identified in this study enable a rapid and efficient identification of the solutes that provide optimum solid–solution strengthening. The approach described here may thus serve as basis for ab initio guided metallurgical materials design.

1. Introduction

Solid solution strengthening is one of the most important strengthening mechanisms. It can be computed using a relatively small set of materials properties, such as the atomic volume, elastic moduli, and/or the stacking fault energy [1–10]. Recent studies [6,8,10] have shown that the solid solution strengthening effect (quantified by the increase in the critical resolved shear stress $\Delta\tau_0$) at the ground state (at $T = 0$ K) can be expressed in terms of two strengthening parameters, namely, the volume misfit parameter, ε_b, and the slip misfit parameter, ε_s. Analytical model approximations for estimating the increase in the critical resolved shear stress $\Delta\tau_0$ normalized by the bulk atomic concentration of solute atoms c are the Nabarro–Labusch model [11–13]:

$$\Delta\tau_0/c^{2/3} = \left(a_1\varepsilon_b^2 + a_2\varepsilon_s^2 + a_3\varepsilon_b\varepsilon_s\right)^{2/3}\ \text{MPa} \tag{1a}$$

and the Friedel–Fleischer model [14,15]:

$$\Delta\tau_0/c^{1/2} = \left(b_1\varepsilon_b^2 + b_2\varepsilon_s^2 + b_3\varepsilon_b\varepsilon_s\right)^{3/2}\ \text{MPa} \tag{1b}$$

The volume misfit parameter ε_b is a measure of an extra volume introduced by a solute atom, and the slip misfit parameter ε_s describes how a specific solute element changes the generalized stacking fault energies. They are defined as

$$\varepsilon_b = \frac{1}{a}\left(\frac{\mathrm{d}a}{\mathrm{d}c}\right)_{c=0} \tag{2a}$$

$$\varepsilon_s = \frac{1}{\gamma}\left(\frac{\mathrm{d}\gamma}{\mathrm{d}c}\right)_{c=0} \tag{2b}$$

where a is the lattice parameter and γ is the generalized stacking fault energy. The slip misfit parameter is conceptually similar to the di-elastic parameter proposed by Fleischer [2,3] who replaced γ in Eq. (2b) by the shear modulus. Both γ and the shear modulus are in principle associated through the shear caused by the dislocations. However, the region close to the dislocation core is characterized by the displacements between two adjacent atomic layers, hence, using the stacking fault energy in this approximation is more pertinent than using the shear modulus in this context.

The numerical constants, i.e. a_i and b_i ($i = 1, 2, 3$) in Eqs. (1a) and (1b) can be obtained by following the procedure discussed in Refs. [6,8,10]. They describe how the volume misfit and the slip misfit interact with the pressure field and the displacement field around a dislocation, respectively. We have followed this procedure in our recent paper [10] and obtained the numerical constants, i.e. a_i in Eq. (1a) (Nabarro–Labusch model) for Al binary

* Corresponding author.
E-mail address: d.ma@mpie.de (D. Ma).

http://dx.doi.org/10.1016/j.actamat.2015.07.054
1359-6454/

solid solutions. In our study [10], the pressure field and the displacement field were obtained by using 2D Peierls–Nabarro model developed as suggested by Schoeck [16,17]. The obtained dislocation–solute interaction energy enters the solid solution strengthening model developed by Leyson et al. [7–9] through the Nabarro–Labusch model. The reason for using Nabarro–Labusch model instead of Friedel–Fleischer model is that it has been shown in [18] that for most cases, when the temperature is above 78 K and the solute concentration is above 0.01 at.%, the Nabarro–Labusch model becomes more appropriate compared to the Friedel–Fleischer model. Thus, considering the Nabarro–Labusch model is likely to be suited for most engineering solid solution alloys.

Employing the above described approach, we had previously performed a parametric study of both, the volume misfit parameter ε_b and the slip misfit parameter ε_s. There are three combinations of a_i $(i = 1, 2, 3)$ depending on the values of ε_b and ε_s. Each combination corresponds to a specific characteristic bow-out distance of the edge dislocation in a metallic matrix with randomly distributed solute atoms (see details in Refs. [7–10]). Eventually, we created a materials-design guideline map of ε_b and ε_s against $\Delta\tau_0/c^{2/3}$ at 0 K. This map is fitted using Eq. (1a). The fitted numerical constants for edge dislocations are listed in Table 1 (specifically for Al solid solutions). With the numerical constants being available, the knowledge of the volume misfit parameter ε_b and the slip misfit parameter ε_s allows for quantitatively predicting the solid solution strengthening effect, as has been demonstrated in [10].

Aiming at a rapid theory-guided alloy prototyping, we below identify compositional trends associated with these two misfit parameters through the whole Periodic table. These trends enable us to estimate the most promising solid solution strengthening elements according to their group numbers in the periodic table relative to the group number of the matrix material. These trends allow us to narrow down the range of possible solute elements before conducting costly and time-consuming experiments or computationally demanding *ab initio* calculations.

First, we focus on Al binary solid solutions which we analyze employing quantum-mechanical calculations. The computational details of the volume and slip misfit parameter of Al binary solid solutions are presented in Section 2. With the results for Al binary solid solutions, we identify compositional trends in the volume and slip misfit parameter as functions of the solutes group number within the Periodic table (Section 3.1). The anti-correlation relationship between the volume and slip misfit parameter observed in Section 3.1 is discussed in Section 3.2. By using the results from Section 3.1, the compositional solid solution strengthening effect will be presented in Section 3.3. Due to the anti-correlation relationship, we show that the solid solution strengthening effect in Al can be roughly estimated by using one misfit parameter, instead of two misfit parameters in Section 3.4. Using the data reported in the literature [6,19–21] we further show similar trends in other binary solid solutions, specifically Mg (basal slip) and Ni (Section 3.5). Our conclusions are drawn in Section 4.

Table 1
Numerical constants used in Eq. (1a) (Nabarro–Labusch model) for edge dislocations in Al binary solid solutions. These numerical constants are taken from [10]. As listed below, there are three combinations of $a_i (i = 1, 2, 3)$ depending on the values of ε_b and ε_s (see Eqs. (2a) and (2b)). Each combination corresponds to a specific characteristic bow-out distance (ω_c) of the edge dislocation in an Al based solid solution with randomly distributed solute atoms. For the definition of ω_c, we refer to [7,8].

	$a_1 \times 10^{-5}$	$a_2 \times 10^{-3}$	$a_3 \times 10^{-3}$
$-0.083 < \varepsilon_b/\varepsilon_s < 0.043$	6.81	3.04	0.18
$-0.193 \leqslant \varepsilon_b/\varepsilon_s \leqslant -0.083$ or $0.043 \leqslant \varepsilon_b/\varepsilon_s \leq 0.123$	5.25	2.04	1.71
else	4.07	1.38	1.80

2. Computational procedure

2.1. Calculation of the volume misfit parameter in Al binary solid solutions

Accurately calculating the volume misfit parameters by *ab initio* methods requires considerable computational resources. First, the volume misfit parameter is defined for solute concentrations approaching zero (see Eq. (2a)) and, therefore, rather large supercells (~100 atoms) with low concentrations of solutes should be used. Unfortunately, quantum-mechanical calculations often scale with the square of the number of atoms in a computational cell. Second, in order to avoid any supercell size dependence of the computed results, a set of different supercells with different sizes should be used [7,8,22]. Both above mentioned aspects render the *ab initio* calculations prohibitively costly. In order to avoid these extensive quantum-mechanical calculations, we adopted a procedure in which we use only medium and small supercell sizes and linearly extrapolate the results to different concentrations. Thanks to the fact that results obtained from these two supercell size sets are clearly linearly related, the compositional dependence of the lattice parameter can be efficiently evaluated without sacrificing much of the required accuracy.

More specifically, to accurately determine the compositional dependence of the lattice parameter, we used two different supercell sizes and five concentrations. The two supercells sizes are $2 \times 2 \times 2$ (32 atoms) and $3 \times 3 \times 3$ (108 atoms) respectively, with the supercells being based on the elementary 4-atomic fcc unit cell in case of the Al matrix. The five concentrations are $Al_{107}X_1$, $Al_{105}X_3$, $Al_{31}X_1$, $Al_{104}X_4$, and $Al_{30}X_2$ (0.926, 2.778, 3.125, 3.704, and 6.250 at.%). All the solute atoms are distributed inside the supercells so as to preserve their overall cubic symmetry. After the lattice parameters were calculated from these concentrations, the composition dependence of the lattice parameter was obtained. Subsequently, we linearly extrapolated the lattice parameter to a higher concentration, namely, 25 at.%. This extrapolated lattice parameter was compared with the calculated lattice parameter by using a $1 \times 1 \times 1$ supercell with a single solute atom in it, Al_3X_1, i.e. with the solute concentration 25 at.%. In order to be representative, we chose Sr, Ca, Ir, Li, Zn, Cu, and Mg as solutes, because (i) the atomic volumes of Sr and Ca are very large compared to the Al atom; (ii) Ir is very small compared to Al; (iii) Li and Zn almost do not change the lattice parameter of Al; while (iv) Cu and Mg moderately change the lattice parameter of Al.

The comparison between the calculated and extrapolated lattice parameters of Al_3X_1 subtracted by the lattice parameter of pure Al $(a_{0,Al})$ is shown in Fig. 1. Our analysis reveals that the calculated lattice parameters are related to the extrapolated ones through a linear function. In order to check the validity of the linear relation, we subsequently performed the same procedure for four other systems, i.e. Al–Si, Al–Cr, Al–Mn, and Al–Fe which are indicated by diamond symbols (◇) in Fig. 1. All these additional data points for these four systems fall approximately on the fitting line. Thus, the volume misfit parameter is approximated by:

$$\varepsilon_b = \frac{a^{extrapo.}_{Al_3X_1} - a_{Al}}{a_{Al}} \times \frac{1}{c} \approx \frac{k \cdot \left(a^{calc.}_{Al_3X_1} - a_{Al}\right)}{a_{Al}} \times \frac{1}{c} \tag{3}$$

where $c = 0.25$, and we chose $k = 1.179$, taking all the data points in Fig. 1 into account. We underline that despite of the fact that the quality of the linear fit in Fig. 1 is excellent ($R^2 = 0.9946$), obtaining ε_b by using Eq. (3) is still only a fair approximation serving our aim

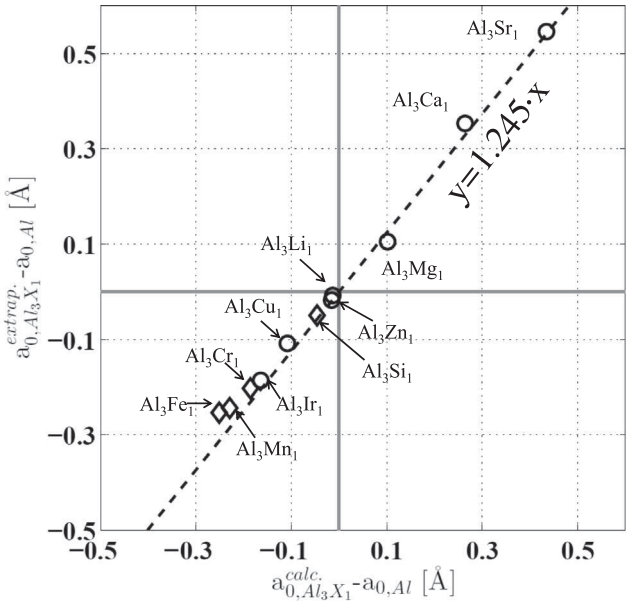

Fig. 1. Calculated lattice parameters of Al_3X_1 ($a^{calc.}_{0,Al_3X_1}$) both subtracted by the lattice parameter of pure Al ($a_{0,Al}$) compared to extrapolated lattice parameters ($a^{extrap.}_{0,Al_3X_1}$) subtracted by the lattice parameter of pure Al ($a_{0,Al}$). $a^{extrap.}_{0,Al_3X_1}$ is obtained by using the compositional dependence of the lattice parameters determined by from larger supercells with low concentrations. The data points indicated by open circle were fitted by a liner function, $a^{extrap.}_{0,Al_3X_1} - a_{0,Al} = k \cdot (a^{calc.}_{0,Al_3X_1} - a_{0,Al})$, where $k = 1.245$. The goodness of fit R^2 is 0.9946 indicating a good fit. The extrapolated and calculated lattice parameters of Al_3Si_1, Al_3Cr_1, Al_3Mn_1, and Al_3Fe_1 (◇, open diamond) were evaluated subsequently, and they all approximately fall on the fitted function. If all the data points, including both ○ and ◇, are used for the fitting, k becomes 1.179 which differ from the original fitted coefficients by −5%.

to compute general trends for indeed numerous solutes across the Periodic table. If only a few specific systems are to be studied, it is still highly recommended that ε_b is evaluated by using larger supercells with lower solute concentrations.

2.2. Calculation of the slip misfit parameter in Al binary solid solutions

Regarding calculations of the slip misfit parameter, we follow the approach proposed by Yasi et al. [6]:

$$\varepsilon_s \approx \frac{1}{\gamma_{I_2,\mathrm{Al}}} \frac{\mathrm{d}\gamma_{I_2,\mathrm{Al\text{-}X}}}{\mathrm{d}c_s} \approx \frac{1}{\gamma_{I_2,\mathrm{Al}}} \frac{\gamma_{I_2,\mathrm{Al\text{-}X}} - \gamma_{I_2,\mathrm{Al}}}{c_s} \tag{4}$$

where the intrinsic stacking fault energy γ_{I_2} is evaluated instead of a generalized stacking fault energy γ used in the original definition of Eq. (2b). The intrinsic stacking fault energy γ_{I_2} is computed for both Al-X matrix-solute alloys (index Al-X) and elemental aluminum (index Al). The intrinsic stacking fault energy is calculated by using the slab model (see e.g., Ref. [23]) with 12 layers of (1 1 1) planes, and the solute atom concentration within the stacking fault plane c_s is 25 %, while the bulk concentration is 2.1%.

2.3. Computational details

All our calculations were performed employing the generalized gradient approximation (GGA-PBE [24]) as exchange–correlation functional and the projector augmented wave (PAW) method [25] as implemented in the VASP code [26,27]. The electronic wave functions were expanded in terms of a plane-wave basis set with an energy cut-off of 420 eV. The reciprocal-space Brillouin zone was sampled using a $24 \times 24 \times 24$ Monkhorst–Pack [28] **k**-point mesh per conventional fcc unit cell for the volume misfit parameter calculations. For the slip misfit parameter, the **k**-point mesh is $20 \times 6 \times 2$. The Fermi surface was smeared by using Methfessel–Paxton smearing method [29] with a smearing parameter $\sigma = 0.4$ eV. The lattice parameters were obtained by fitting the energy–volume curves using the Birch–Murnaghan equation of state [30,31].

Our study does not cover all possible solutes from the whole periodic table. Focusing on substitutional solid solutions, we excluded a few light elements (H, He, C, N, O and F) that are unlikely to substitute atoms in common metallic matrices. Our calculations were conducted without considering spin polarization of atoms, i.e. all simulations are non-magnetic, including 3d elements (Cr, Mn, Fe, Co and Ni) that are ferro- and anti-ferro-magnetic in their elemental ground states. This seemingly crude simplification is motivated by the fact that, e.g., low-concentration Fe atoms dispersed in Al matrices have been shown to have their local magnetic moments reduced to 10% of the magnetic moments in the elemental bcc Fe (see, e.g., Ref. [32]). Therefore, we expect the magnetism of these solutes to be absent or weak in case of the low solute concentrations that can be obtained in Al based alloys. Lastly, we have also omitted some radioactive elements in the 6th period (Po, At and Rn), lanthanides, and 7th period elements.

3. Results and discussion

3.1. Volume and slip misfit parameters in Al solid solutions

Fig. 2(a) shows the calculated volume misfit parameters of Al binary solid solutions using Eq. (2a) plotted against the group number of the solute elements. For solute elements belonging to a single period, the predicted dependence of the volume misfit parameter vs. group number follows a convex trend. The parabolic trends have minimum values for either the group 9 (in case of the 4th period) or the group 8 (in case of 5th and 6th periods). The noble gas and alkaline metals cause the largest volume expansion, and the middle transition metals, e.g. groups 8 or 9, introduce the largest volume contraction. From group 13 to group 15 (e.g. Ga, Ge, As), the slope is changing as the lattice parameter is not increasing as steeply as in case of other groups. If the solute elements are in the same group of the 5th and 6th period, the volume misfit parameters are close to each other, except Y and La. A very similar trend was also recently obtained in a study in which larger supercells were used (see Fig. 9 in Ref. [33]).

The above summarized findings mostly agree with trends observed for the atomic volumes measured from the pure substances in the 4th, 5th and 6th periods [34]. This means that the trend of the volume misfit parameter can be approximated by Vegard's law, i.e.

$$a_{\mathrm{Al}_{1-c}\mathrm{X}_c} = (1-c) \cdot a_{\mathrm{Al}} + c \cdot a_{\mathrm{X}} \tag{5}$$

where $a_{\mathrm{Al}_{1-c}\mathrm{X}_c}$, a_{Al} and a_{X} are the lattice parameters of the solid solution, pure Al, and pure solute assuming fcc structure, respectively; c is atomic concentration. Quantitatively, however, Vegard's law deviates from the DFT calculations and there is also an issue connected with solutes taken from group number higher than 12. If empirical atomic radii as proposed by Slater [35] are used as references for a_{X} in Eq. (5) employing the Vegard's law, the lattice parameter as a function of the group number would assume a local maximum at group 12 or 13. Apparently this is not the case in Al binary solid solutions (see Fig. 2(a)). In Mg and Ni binary systems, however, Slater's atomic radius approximation works better, because there is a local maximum at group 12 in some periods (see below in Section 3.5).

Fig. 2(b) shows the slip misfit parameter of Al binary solid solutions vs. the group number of the corresponding solute elements.

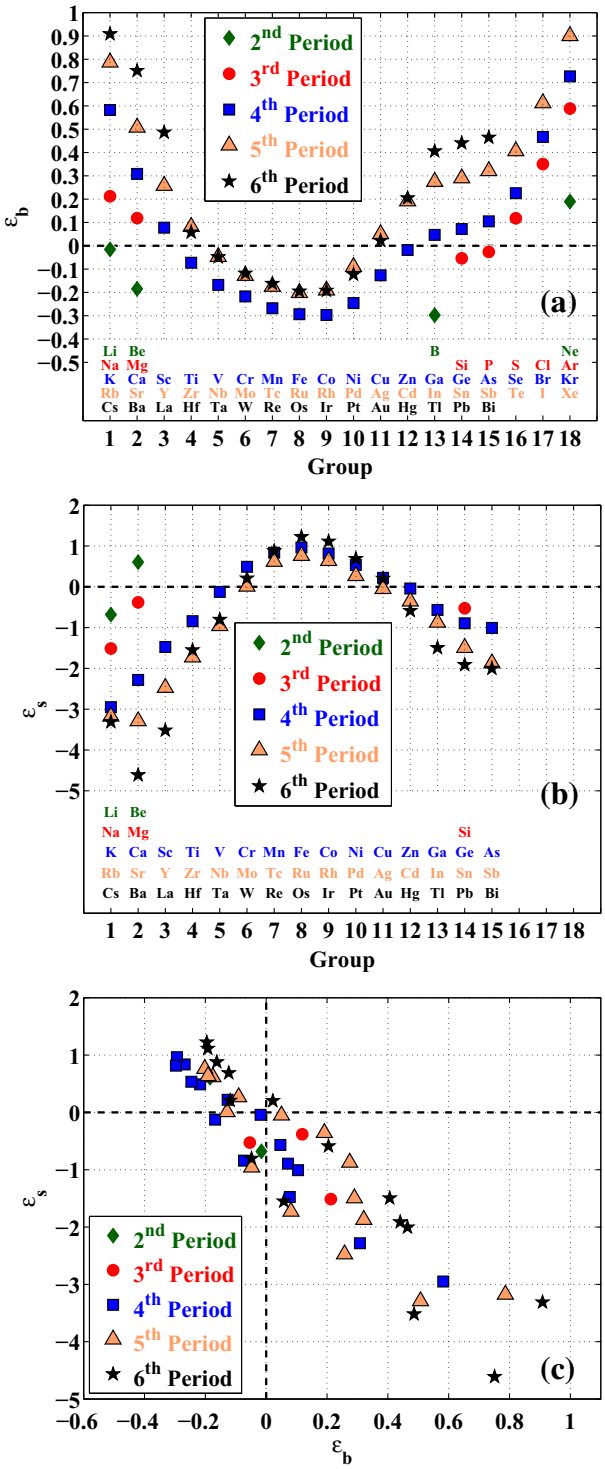

Fig. 2. (a) The volume misfit parameter (ε_b) of Al based binary alloys using Eq. (3). (b) The slip misfit parameter (ε_s) of Al based binary alloys using Eq. (4). (c) Correlation between ε_b and ε_s.

In contrast to the volume misfit parameter, within a single period, the slip misfit parameters usually follow a concave trend.

3.2. Anti-correlation relation between volume and misfit parameter

Comparing Fig. 2(a) and (b) the volume misfit and slip misfit parameters seem to be inversely related in Al binary solid solutions, namely, the higher the volume misfit parameter, the lower is the slip misfit parameter. The level of anti-correlation can be quantified by evaluating the sample correlation coefficient r. For two data sets ε_b^i and ε_s^i, this coefficient is defined as:

$$r = \frac{n\sum_{i=1}^{n}\varepsilon_b^i\varepsilon_s^i - \sum_{i=1}^{n}\varepsilon_b^i\sum_{i=1}^{n}\varepsilon_s^i}{\sqrt{n\sum_{i=1}^{n}\varepsilon_b^{i2} - \left(\sum_{i=1}^{n}\varepsilon_b^i\right)^2}\sqrt{n\sum_{i=1}^{n}\varepsilon_s^{i2} - \left(\sum_{i=1}^{n}\varepsilon_s^i\right)^2}} \tag{6}$$

Specifically in case of the volume misfit and slip misfit parameters ε_b^i and ε_s^i (visualized in Fig. 2(c)) the corresponding value of the sample correlation coefficient r is -0.92 indicating very strongly anti-correlated quantities. In order to test the robustness of the anti-correlation relationship, we randomly took one data point out from Fig. 2(c) and the value of the sample correlation coefficient r was found to vary only by $\sim\pm0.7\%$.

The anti-correlation relation between the volume misfit and slip misfit in Al binary solid solutions can be qualitatively understood from the topology of the charge density in Al. It stems from the fact that the slip misfit parameter is closely related to the intrinsic stacking fault energy, and this property is related to the topology of the charge density (see, e.g., Ref. [36]). In pure Al, it has been observed that the average charge density in the tetrahedral interstitial site in the fcc structure is much larger than that in octahedral interstitial lattice sites [36], and this inhomogeneous charge density distribution is attributed to the high intrinsic stacking fault energy of Al [36–38]. The charges in the tetrahedral interstitial site are associated with the electrons near the Fermi level, hence it can be assumed that lowering the Fermi level in Al would lead to a more homogeneous charge distribution [36], which results in a lower stacking fault energy. If we plot the slip misfit parameter against the compositional dependence of the Fermi energy of selected Al binary systems, as shown in the left-hand part of Fig. 3, the slip misfit parameter is indeed correlated with the Fermi level in such a way that the higher the Fermi level the higher the slip misfit parameter or, in other words, the higher the Fermi level, the higher the intrinsic stacking fault energy.

The connection between the volume and the Fermi level shift can be qualitatively understood within the free electron model in which the Fermi level is related to the density of electrons [39]:

$$E_F \propto \left(\frac{N}{V}\right)^{2/3} \tag{7}$$

where E_F is the Fermi energy; N is the number of electrons, and V is atomic volume. In pure metals, when N is a constant, it has been shown that the larger the volume the lower the intrinsic stacking fault energy in Al, Ni and Cu [38,40]. This is consistent with a proposal by Kioussis et al. [36] who suggested that bringing down the Fermi level lowers the intrinsic stacking fault energy. In solid solutions, the Fermi level shift is due to a competition between the number of the valence electrons of the solute element and the volume change caused by the solute element. Within the rigid band model (ignoring the volume), all the solute elements in Fig. 3 should lower the Fermi level, because all the solute elements have less valence electrons than Al. This indeed applies here for most of the selected elements, except for Ir, because Ir introduces a larger volume contraction, hence the Fermi level is increased by Ir. In the case of Li and Zn, their volume effects are comparable (almost the same ε_b), but Li lowers the Fermi level more than Zn. This is due to the fact that Zn has 2 valence electrons and Li has only one (considering that Al has 3 valence electrons). Apart from that, the volume effect seems to play a larger role in shifting the Fermi level in Al than the number of the valence electrons.

This analysis suggests that the anti-correlation between the volume misfit and the slip misfit comes from the fact that the increased volumes lead to a reduction of the Fermi level, which in turn lowers the intrinsic stacking fault energy. It should be

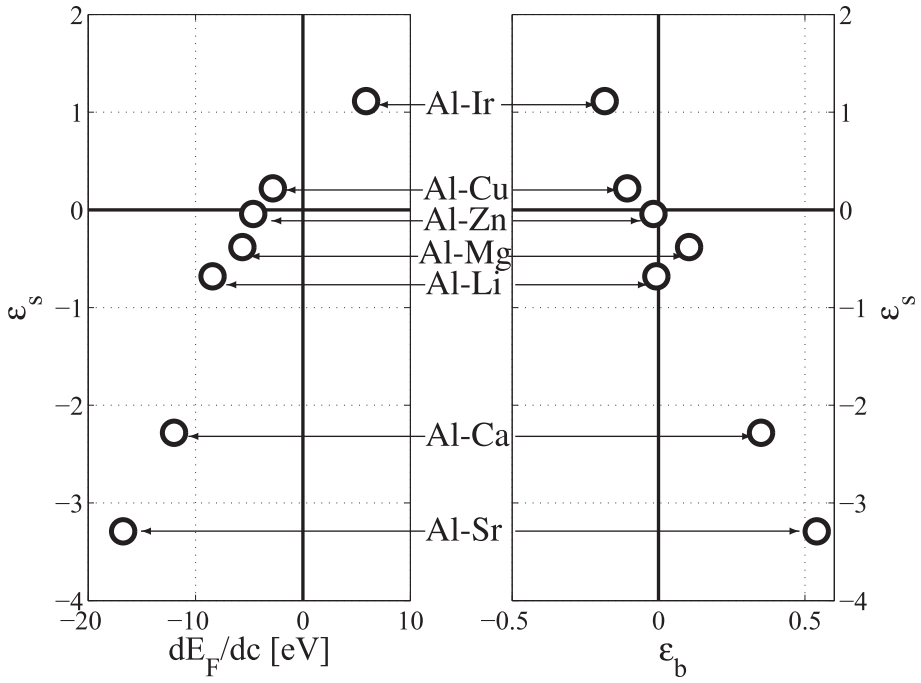

Fig. 3. The slip misfit parameter (ε_s) as a function of (left) the compositional dependence of the Fermi energy (dE_F/dc), or (right) volume misfit parameter (ε_b). The Fermi energies are from the calculations with full relaxation, including volumetric and atomic relaxation. It should be noted that ε_b in the right are from the calculations with large supercells (see Section 2.1).

noted, that the data points in Fig. 3 do not pass through the origin. This means that lowering the Fermi level does not necessarily lower the intrinsic stacking fault energy. The reason for that is not quite clear yet and beyond the scope of this study. We attribute this minor inconsistency to the fact that the above discussion connecting the volume effect to the intrinsic stacking fault energy is based on the free electron model which is only an approximation. We admit that, e.g., charge transfers during the stacking fault formation are very complicated processes [36] and a single parameter, like the Fermi level, might not be sufficient to determine its energetics. It is also true that the charge density in Al is not homogeneously distributed. It was, nevertheless, shown that the electron density of states in Al (both in a perfect fcc crystal or a crystal with stacking faults) is close to that predicted by the free electron model which thus offers a sufficiently good description for the case of Al [38]. The free electron model can provide a deeper qualitative understanding of the observed anti-correlation between the volume misfit and slip misfit parameter.

3.3. Compositional strengthening effect and suggestions for effective strengtheners

Having identified the compositional trends in the misfit parameters in Al, we next use them as input for Eq. (1a) and analyze their impact on solid–solution strengthening. We use the misfit parameters ε_b and ε_s in Fig. 2(a) and (b), together with Eq. (1a) (Nabarro–Labusch model) and the numerical constants listed in Table 1 as taken from Ref. [10]. The computed compositional dependences of the increase in the critical resolved shear stress $\Delta\tau_0$ (scaled by the solute concentration c) at 0 K are shown in Fig. 4.

Within each of the periods shown in Fig. 4, the elements showing a poor solid–solution strengthening capacity can be found in groups 4, 5, 11, and 12 where the misfit parameters approach zero (see Fig. 2(a) and (b)). Note that they are near group 13 where the matrix element Al is located too, and group 18–13 (maximum group number 18 minus the group number of Al). The most

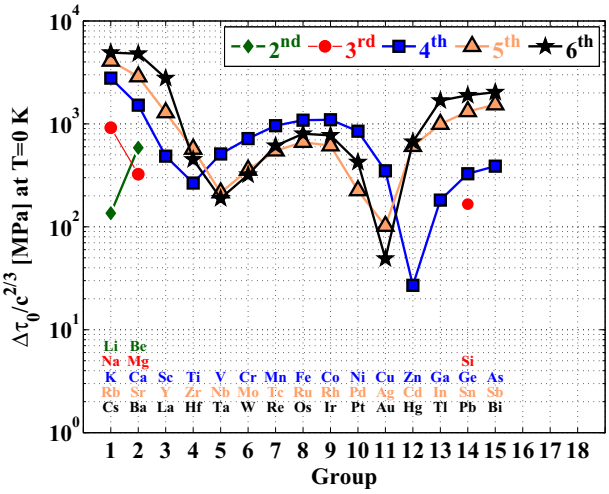

Fig. 4. The predicted value of $\Delta\tau_0$ (the increase in the critical resolved shear stress) scaled by $c^{2/3}$ at 0 K of Al binary solid solutions, where c is the concentration. Abscissa: group number of the solute element. The lines here are used to guide your eyes. $\Delta\tau_0/c^{2/3}$ are obtained by inserting the misfit parameters (ε_b and ε_s) in Fig. 2(a) and (b) into Eq. (1a) (Nabarro–Labusch model), together with the numerical constants shown in Table 1 from Ref. [10] in which the solid solution strengthening model developed by Leyson et al. [7,8] was employed.

effective solid solution strengtheners are found around group 1 (alkali metal), group 9 in Period 4, 5, 6. The strengthening capabilities of particularly these effective strengtheners are, however, of limited interest owing to their low solubility in Al. A possible route to overcome this limitation is to use special metallurgical processes to obtain supersaturated solutions, such as rapid quenching from the melt, by using which, for example, 10 at.% Mn in Al in solid solution state can be achieved, while its maximum solubility is only 0.62 at.% at 931 K [49]. Another limiting factor is thus diffusion, because a slow diffusion would stabilize the supersaturated solid solution, rather than forming precipitates. As shown in

Ref. [50], the diffusion rate of the solute elements around group 1 in Al is determined by the Al-vacancy exchange energetics (formation energy of the vacancies and mobility barrier). Therefore, the activation energy for diffusion of these elements in Al is close to (or lower than) that of the Al self-diffusion. The elements around group 9 strongly repel the vacancies in Al and the diffusion rate is determined by the solute-vacancy exchange. Consequently, the diffusion activation energy of these elements in Al is much larger than that of Al self-diffusion. According to this consideration of diffusion, the elements around group 9 would be more effective solid solution strengtheners than the ones around group 1.

Another important aspect of our analysis is the temperature. The increase in the critical resolved shear stress $\Delta\tau_0$, i.e. the stress to overcome the energy barrier (ΔE_b) against dislocation motion, is shown in Fig. 4 for $T = 0$ K. At finite temperatures, the dislocation motion can be supported by thermal activation, and ΔE_b can be thermally overcome. The thermal activation process can be described by using the theory developed by Kocks et al. [51,52]. As shown in Ref. [8,10], ΔE_b can be also expressed similarly to $\Delta\tau_0$ at $T = 0$ K in terms of ε_b and ε_s, of course with different numerical constants and a different concentration scaling. The general trend of $\Delta\tau_0$ at finite temperatures with respect to the group number is thus the same as shown in Fig. 4.

It should be noted that despite the fact that the range of ε_s is one order of magnitude higher than that of ε_b (see Fig. 2(a) and (b)), the numerical constants before ε_s listed in Table 1 are lower than those before ε_b by two orders of magnitude. This means that the contribution of ε_s is one order of magnitude lower than that of ε_b. Ignoring the contribution of ε_s and the cross term $\varepsilon_b \cdot \varepsilon_s$ in Eq. (1a), the evaluated values for the available strengthening product term $\Delta\tau_0/c^{2/3}$ is lowered by 19 % on average with a standard deviation of 22 %. A more detailed discussion of these aspects can be found in, e.g., our recent paper [10].

3.4. Reducing two strengthening parameter into one strengthening parameter as number of merit

Due to the strong anti-correlation of the volume and slip misfit parameters shown in Section 3.2, Eq. (1a) or Eq. (1b) may be further reduced to a single-variable function using either ε_b or ε_s. We approximate ε_s in terms of ε_b using a linear function

$$\varepsilon_s = K \cdot \varepsilon_b \tag{8}$$

and Eq. (1a) is transformed to

$$\Delta\tau_0/c^{2/3} = A \cdot \varepsilon_b^{4/3}\ \text{MPa}, \tag{9}$$

where

$$A = \left(a_1 + a_2K^2 + a_3K\right)^{2/3}. \tag{10}$$

Studying Al solid solutions, we use the numerical constants $(a_i, i = 1,2,3)$ from Table 1, and $K = -4.216$ which provides the best fit to Fig. 2(c). We then arrive at A = 8137, 6747, or 5640, depending on the values of ε_b and ε_s. In [8], a single parameter (ΔV_m, the extra volume introduced by the solute atom in a matrix) is used to express $\Delta\tau_0/c^{2/3}$, similarly to Eq. (9). In order to compare these two approaches with different parameters, we consider that $V_m = a^3/4$, where 4 means that there are 4 atoms in fcc unit cell, then $\Delta V_m = (3a^2/4)(\mathrm{d}a/\mathrm{d}c) = (3a^3/4)((1/a)(\mathrm{d}a/\mathrm{d}c)) = (3a^3/4)\varepsilon_b$. With this knowledge we convert ε_b to ΔV_m and the pre-factor becomes 44.8, 37.2, or 31.1 Å^{-4}, among which the last one perfectly matches the value of 31.1 Å^{-4} obtained in [8]. It should be also noted that in Ref. [8], the solute elements Mg, Cu, Cr, Mn, Fe, Si in Al were studied. The misfit parameters of Mg, Cu, Cr, Mn, Fe in Al fall in the range that the numerical constants of $a_1 = 4.07 \times 10^5, a_2 = 1.38 \times 10^3, a_3 = 1.80 \times 10^3$ should be used (see Fig. 2(b) and Table 1). These numerical constants (a_i, (i = 1,2,3)) give the prefactor of 31.1 Å^{-40} in Eq. (9), if ε_b is converted to ΔV_m in Eq. (9). It is worth mentioning that in Refs. [7,8], ε_s was not considered as a material property correlating with the solid solution strengthening, but the contribution of the slip misfit to the strengthening was implicitly included in the dislocation–solute interaction energy calculation by *ab initio* method. Therefore, using single parameter expression as a trend measure for "solid solution merit" still provides an acceptable fit as shown in Ref. [8], and the contribution of the slip misfit is hidden by the anti-correlation relation between the volume misfit and the slip misfit.

The anti-correlation relation and the single-parameter fit certainly provide an advantage for estimating the solid solution strengthening because ε_s, which is difficult to measure and calculate, can be replaced by ε_b which is relatively easy to measure and/or calculate. One should, however, take caution when applying this anti-correlation relation. Even though ε_b and ε_s are strongly anti-correlated, they still exhibits a certain scatter. Thus, Eq. (8) is still only an approximation, and Eq. (9) gives a error of ~±500 MPa, roughly 20% of the prefactor, A. Nevertheless, this anti-correlation relation is perfectly sufficient for the purpose of our study in which we aim at general trends.

3.5. Volume and slip misfit parameters in other systems with low Peierls stress of matrices

Our study has been so far focusing on compositional trends in misfit parameters in Al-based binary solid solutions that we got from quantum-mechanical calculations. Next, we search for similar trends (and their anti-correlations) in other solid solutions with matrices possessing low Peierls potentials (e.g. fcc crystals and basal slip in hcp metals). Our choice of systems is motivated by the fact that the limiting factors for dislocation motion in metals with high Peierls potentials (such as bcc metals) are different from those in an Al matrix, i.e. the core structure of the screw dislocation and the nucleation and migration of the kink-pairs. The solute atoms can change the core structure of the dislocations [41], or promote nucleation and migration of the kink-pairs [42], entailing solid solution softening.

Focusing on systems with low Peierls potentials, we have re-analyzed the reported data which include: (1) *ab initio* calculations of ε_b and ε_s in case of basal slip in Mg binary systems [6], (2) the lattice parameters of Ni binary solid solutions determined by experiments [19] and *ab initio* calculations [20], and the intrinsic stacking fault energy obtained by ab initio calculations [21]. The re-analyzed data are shown in Fig. 5.

In Mg binary solid solutions, the volume misfit parameters related to the basal slip again follow a convex trend, except for a few elements (see Fig. 5(a)). As we are using data published by other groups it should be noted that the volume misfit parameter calculated in Ref. [6] is based on a definition that is different from the one used in this study. In Ref. [6], it is calculated by using the concept of the strength of the point defect as originally proposed by Eshelby [43]. The volume misfit parameter in Eq. (2a) was originally proposed by Cottrell [1] which is derived only from geometrical quantities, such as the lattice parameter or the atomic volume. For the slip misfit parameter, the trend is concave except in the 2nd period (Fig. 5(c)).

In Ni binary solid solutions (Fig. 5(b)), the volume misfit parameters also follow a convex trend for the 5th and 6th periods from group 3 (or 4) to 12. Starting from group 12 (or 13), the volume misfit parameter decreases as the group number increases in the 3rd, 4th and 5th period. This feature resembles the trend of theoretically determined empirical atomic radii [35] where the atomic

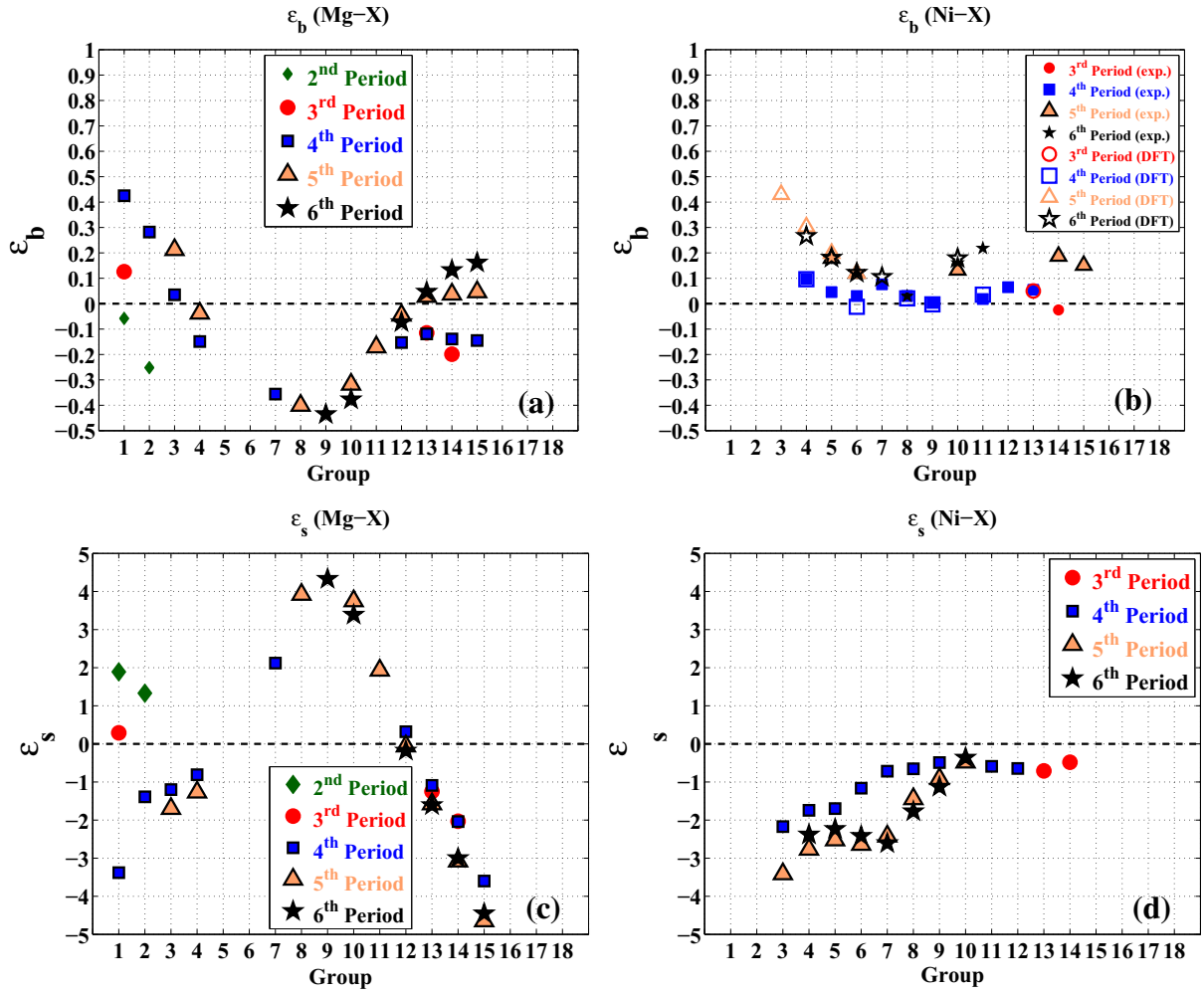

Fig. 5. Volume misfit parameters ε_b (a), (b) and slip misfit parameters ε_s (c), (d) as functions of the group number of the solute element in Mg binary solid solutions (a), (c) and Ni binary solid solutions (b), (d). The above figures are plotted by re-analyzing the data from Ref. [6] (Mg-X) and Ref. [19–21] (Ni-X).

radius decreases as the group number increases starting from group 12. When Ni is alloyed with 3d magnetic elements, the convex trend is violated, too, especially for Mn (group number 7), due to different volume in magnetic elements cause by their magnetic polarization.

The slip misfit parameters of Ni binary solid solutions are shown in Fig. 5(d). In general, the concave trend is again followed, but in the 5th and 6th periods local minima can be found in groups 6 and 7. Besides the evidence from the theoretical calculations [21] shown in Fig. 5(d), the concave shape of the slip misfit parameter in Ni binary systems is also evident in measured intrinsic stacking fault densities [44]. According to these measurements the ability of a solute to increase the intrinsic stacking fault density follows this sequence (from strong to weak): Ti(4), Mo(6), W(6), V(5), Cr(6), Mn(7), Co(9), Cu(11), Fe(8), where the group numbers are indicated in round brackets. Considering that: (i) the group number of Ni is 10, (ii) the increase in the stacking fault density is a consequence of the decrease of the stacking fault energy, we can conclude that the ability of a solute to decrease the intrinsic stacking fault energy follows the sequence of the ability of increasing the intrinsic stacking fault density. Therefore, the slip misfit parameter decreases as the group number of the solute element deviates from 10, i.e. from the group number of the Ni matrix.

Next to the above two systems, indirect experimental evidence indicates that the concave trend of the slip misfit parameters is also valid in other fcc solid solutions, e.g. Cu and Ag. It was shown in Ref. [45] that (i) the stacking fault energies in Cu and Ag based binary solid solutions decrease as the alloy concentration increases, and (ii) the higher the electron-atom ratio, the lower the stacking fault energy. These observations were, however, based on the Cu and Ag based binary solid solutions in which the solute elements have all higher group numbers than Cu and Ag (they are located on the right-hand side with respect to Cu and Ag in the periodic table). This means, that the capability of the solute in decreasing the stacking fault energy of Cu and Ag increases, as the group number of the solute increases starting from 11 (Cu and Ag are in group 11), which is consistent with the concave trend.

Analyzing mutual inter-relations between both misfit parameters, the sample correlation coefficients r from Eq. (6) have been computed to be −0.73 and −0.74 for Mg-X (basal slip) and Ni-X, respectively, which indicates anti-correlation relations between ε_b and ε_s. When only comparing the coefficients, r, it appears that the anti-correlation relations in Mg-X and Ni-X are not as strong as that in Al-X ($r = -0.92$). It should be noted that if we again randomly take out one data point, value of r varies ±5.5% for Mg-X, and ±12% for Ni-X, while it is ±0.7% for Al-X. Therefore, there might not be sufficient data points for Mg-X and Ni-X to reliably assess the level of anti-correlation. Another aspect is that in Mg-X ε_b and ε_s are not so strongly anti-correlated as in Al-X

because (i) when the solute elements are from the 2nd period, i.e. Li and Be, this anti-correlation relation is clearly violated, (ii) and after reaching a maximum at group 13 in the 3rd and the 4th period, ε_b starts to decrease, but ε_s continues to decrease. As discussed in Section 3.1, the feature of having a maximum at group 13 in ε_b follows the trend of Slater's empirical atomic radius [35]. In contrast to that in Al-X, ε_b does not follow the trend of Slater's empirical atomic radius but, instated, the trend of the atomic volume measured from pure substances.

Another important mechanism is the charge transfer that has been shown in pure Mg to operate similarly as in pure Al during stacking fault formation [46]. A similar relation between the Fermi level and the intrinsic stacking fault energy (see Fig. 3) is, however, not valid, when comparing Li and Al in Mg [46]. Han et al. [46] have shown that the Fermi level of Mg–Al is higher than that of Mg–Li, but the intrinsic stacking fault energy on basal slip of Mg–Al is lower than that of Mg and Mg–Li (also see Fig. 5(a) and (c)). As mentioned above, the concave trend of the slip misfit parameter in Mg binary systems is only violated in the 2nd period where Li is located, therefore, comparing Al and Li in Mg might not be representative. Since Mg is also a simple metal, the free electron model can be used as an approximation as for Al, too. Therefore, we assume for Mg alloys (similarly as for Al alloys) that the volume and slip misfit parameters are anti-correlated because of the Fermi level shift caused by the volumetric effect.

As for Ni, the charge distributions in fcc metals are topologically very similar to each other [47,48], and the mechanism of the charge redistribution during the stacking fault formation has been found to be very similar also among Al, Cu, and Ir, therefore we expect it also to hold for Ni. Our explanation to the anti-correlation relation between ε_b and ε_b in Ni binary systems may follow the line of Al binary systems (see the end of Section 3.1). The only difference might be that d-electrons are more localized than s-p electrons. Therefore, similar to pure Cu, the charge distribution in Ni is less directional and more homogeneous than that in Al. Consequently, the slip misfit parameters of Ni binary solid solutions are not very sensitive to alloying compared with Al and Mg binary solid solutions (see Figs. 2(b) and 5(c) and (d)). It is also observed that the stacking fault energies in both pure Cu and Ni are not sensitive to the volumetric change [38].

If we assume the underlining solid solution strengthening mechanism is the same in the systems where the Peierls potentials of the matrices are low, such as fcc and basal slip in hcp. Following the procedure in [6,8,10], one should be able to obtain the numerical constants for Eq. (1a), for Ni and Mg (basal slip) binary systems.

Once these numerical constants in Eq. (1a), for Ni and Mg (basal slip) binary systems are obtained, following the trends shown in Figs. 2, 5 and 4, the position of the solute elements of the least strengthening capability can be identified at points where $\varepsilon_b = 0$ and $\varepsilon_s = 0$. According to Figs. 2 and 5, the values corresponding to $\varepsilon_b = 0$ and $\varepsilon_s = 0$ can be found approximately around the group number of the matrix G_{matrix} and 18-G_{matrix}, where G_{matrix} is the group number of the matrix element. As shown in Fig. 4, very effective strengtheners can be found in groups 1 (alkali metals) and group 9. When the solute elements have their group number higher than 12, i.e. entering the main groups, caution should be taken since the trend could deviate severely from the anti-correlation relation between ε_b and ε_s as shown in Figs. 2 and 5(a) and (b).

It is should be noted that dislocations dissociate more in Mg (basal slip) and Ni than in Al, due to their low stacking fault energies than Al. Consequently, in a solid solution with randomly distributed solute atoms, such as in Mg–Al [9], the dislocations may have multiple configurations, i.e. bow-out shapes. Different dislocation configurations correspond to different energy barriers against dislocation motions, hence causing different critical resolved shear stresses, and different configurations associated with different energy barriers prevail over the others in different temperature ranges. Despite of that, for a specific temperature range, the above generalized trends of strengthening capabilities of the solute elements should still be valid.

4. Summary

We have used quantum-mechanical calculations to identify compositional trends in the volume and slip misfit parameters using Al binary solid solutions as a model case. The volume misfit parameter (ε_b) follows a convex trend as a function of the solute group number in the Periodic table. In contrast, the slip misfit parameter (ε_s) follows a concave shape. The only exception are solutes beyond the group 12, i.e. leaving the transition metal group and entering the main group. In Al binary solid solutions, ε_b and ε_s are found to be strongly anti-correlated. This findings enables us to identify a single-parameter description of solid solution strengthening as we illustrate using the volume misfit parameter (solid solution strengthening measure of merit). The anti-correlation has been qualitatively explained in terms of the Fermi level shift caused by the volume change associated with the respective solutes.

Having the compositional trends, the solid solution strengthening capability of the different solutes in Al has been evaluated. Elements showing rather poor solid–solution strengthening capabilities have minimum volumetric misfit. They are mostly from group 4, 5, 11, and 12, i.e. close to the group of the matrix (here Al) or from the group with the group number that – when added to the group number of the matrix – gives 18. The elements with maximum solid solution strengthening capability can be found around groups 1 and 9. Based on additional considerations regarding the diffusion of group 1 and group 9 elements in Al, we suggest that the most effective solid solution strengtheners should be group 9 elements for the Al model alloy case.

Using previously published data from the literature we identify qualitatively identical compositional trends (convex volume misfit parameter and concave slip misfit parameter) also in Mg (basal slip) and Ni binary solid solutions. We believe that our findings can be generalized and applied to the strengthening capability of solutes also in other systems with low Peierls potentials. We thus conclude that the elements showing poor solid solution strengthening capabilities have a group number close to (i) that of the matrix G_{matrix} and (ii) 18-G_{matrix}, where G_{matrix} is the group number of the matrix element. Caution should be taken when the group number of the elements is higher than 12. The above identified trends and anti-correlations in the misfit parameters can serve as a guideline within a future theory-guided materials design when identifying optimal solutes that provide an application oriented solid solution strengthening for a given matrix.

Acknowledgements

D.M expresses his gratitude to Dr. Gerard Leyson for his careful and thorough reading our manuscript and providing his insightful and fruitful comments. M.F. acknowledges financial support from the Academy of Sciences of the Czech Republic through the Fellowship of Jan Evangelista Purkyně and the access to the computational resources provided by the MetaCentrum under the program LM2010005 and the CERIT-SC under the program Centre CERIT Scientific Cloud, part of the Operational Program Research and Development for Innovations, Reg. No. CZ.1.05/3.2.00/08.0144.

References

[1] A. Cottrell, Effect of solute atoms on the behaviour of dislocations, in: Report on Conference of the Strength of Solids, Physical Society, London, UK, 1948, pp. 30–37 (Conference on the strength of solids, 1947, London, UK).

[2] R.L. Fleischer, Solution hardening, Acta Metallur. 9 (11) (1961) 996–1000, http://dx.doi.org/10.1016/0001-6160(61)90242-5. <http://www.sciencedirect.com/science/article/B7598-48GX9HM-PH/2/b341350225d5e6c32aa5ea712ed70c38>.

[3] R.L. Fleischer, Substitutional solution hardening, Acta Metallur. 11 (3) (1963) 203–209, http://dx.doi.org/10.1016/0001-6160(63)90213-X. <http://www.sciencedirect.com/science/article/B7598-48HRX1X-11D/2/ed64972f851ecece8dcb4aacc25a0f39>.

[4] R. Bullough, R.C. Newman, The kinetics of migration of point defects to dislocations, Rep. Progr. Phys. 33 (1) (1970) 101–148. <http://stacks.iop.org/0034-4885/33/i=1/a=303>.

[5] P. Haasen, Solution hardening in f.c.c. metals, in: F.R.N. Nabarro (Ed.), Dislocations in Solids, Dislocations in Metallurgy, vol. IV, North-Holland, Amsterdam, Netherlands, 1979, pp. 155–189.

[6] J.A. Yasi, L.G. Hector Jr., D.R. Trinkle, First-principles data for solid–solution strengthening of magnesium: from geometry and chemistry to properties, Acta Mater. 58 (17) (2010) 5704–5713, http://dx.doi.org/10.1016/j.actamat.2010.06.045. <http://www.sciencedirect.com/science/article/B6TW8-50JKNDY-4/2/98af5b372f11546453cf64f45f39670b>.

[7] G.P.M. Leyson, W.A. Curtin, L.G. Hector Jr., C.F. Woodward, Quantitative prediction of solute strengthening in aluminium alloys, Nature Mater. 9 (9) (2010) 750–755, http://dx.doi.org/10.1038/nmat2813. <http://www.nature.com/nmat/journal/v9/n9/full/nmat2813.html>.

[8] G.P.M. Leyson, L.G. Hector Jr., W.A. Curtin, Solute strengthening from first principles and application to aluminum alloys, Acta Mater. 60 (9) (2012) 3873–3884, http://dx.doi.org/10.1016/j.actamat.2012.03.037. <http://www.sciencedirect.com/science/article/pii/S1359645412002273>.

[9] G.P.M. Leyson, L.G. Hector Jr., W.A. Curtin, First-principles prediction of yield stress for basal slip in Mg–Al alloys, Acta Mater. 60 (13–14) (2012) 5197–5203, http://dx.doi.org/10.1016/j.actamat.2012.06.020. <http://www.sciencedirect.com/science/article/pii/S1359645412003928>.

[10] D. Ma, M. Friák, J. von Pezold, D. Raabe, J. Neugebauer, Computationally efficient and quantitatively accurate multiscale simulation of solid–solution strengthening by ab initio calculation, Acta Mater. 85 (0) (2015) 53–66, http://dx.doi.org/10.1016/j.actamat.2014.10.044. <http://www.sciencedirect.com/science/article/pii/S1359645414008088>.

[11] R. Labusch, A statistical theory of solid solution hardening, Phys. Status Solidi (b) 41 (2) (1970) 659–669, http://dx.doi.org/10.1002/pssb.19700410221. <http://dx.doi.org/10.1002/pssb.19700410221>.

[12] R. Labusch, Statistische theorien der mischkristallhärtung, Acta Metall. 20 (7) (1972) 917–927, http://dx.doi.org/10.1016/0001-6160(72)90085-5. <http://www.sciencedirect.com/science/article/B7598-48K6WPC-D4/2/e329ba3c98ea75448b1c423159e058fa>.

[13] M. Zaiser, Dislocation motion in a random solid solution, Philos. Mag. A 82 (15) (2002) 2869–2883. <http://www.informaworld.com/10.1080/01418610208240071>.

[14] J. Friedel, Dislocations, Pergamon, Oxford, 1961.

[15] R.L. Fleischer, Solid–solution hardening, in: D. Peckner (Ed.), The Strengthening in Metals, New York, Reinhold Press, 1964, pp. 93–140 (Chapter 3).

[16] G. Schoeck, The core structure, recombination energy and peierls energy for dislocations in Al, Philos. Mag. A 81 (5) (2001) 1161–1176, http://dx.doi.org/10.1080/01418610108214434. <http://www.tandfonline.com/doi/abs/10.1080/01418610108214434>.

[17] G. Schoeck, The Peierls model: progress and limitations, Mater. Sci. Eng.: A 400–401 (0) (2005) 7–17, http://dx.doi.org/10.1016/j.msea.2005.03.050. <http://www.sciencedirect.com/science/article/pii/S0921509305002704>.

[18] G.P.M. Leyson, W.A. Curtin, Friedel vs. Labusch: the strong/weak pinning transition in solute strengthened metals, Philos. Mag. 93 (19) (2013) 2428–2444, http://dx.doi.org/10.1080/14786435.2013.776718.

[19] W. Pearson, Handbook of Lattice Spacings & Structures of Metals & Alloys, International Series of Monographs on Metals Physics & Physical Metallurgy, vol. 411, Franklin Book Co, 1964, ISBN 0080090788. <http://www.amazon.com/Handbook-Structures-International-Monographs-Metallurgy/dp/0080090788>.

[20] D. Kim, S.L. Shang, Z.K. Liu, Effects of alloying elements on elastic properties of Ni by first-principles calculations, Comput. Mater. Sci. 47 (1) (2009) 254–260, http://dx.doi.org/10.1016/j.commatsci.2009.07.014. <http://www.sciencedirect.com/science/article/B6TWM-4X2BV39-2/2/e9b1a9c16e95fa3384f500952506a669>.

[21] S.L. Shang, C.L. Zacherl, H.Z. Fang, Y. Wang, Y. Du, Z.K. Liu, Effects of alloying element and temperature on the stacking fault energies of dilute ni-base superalloys, J. Phys.: Condens. Matter 24 (50) (2012) 505403. <http://stacks.iop.org/0953-8984/24/i=50/a=505403>.

[22] S. Vannarat, M.H.F. Sluiter, Y. Kawazoe, First-principles study of solute-dislocation interaction in aluminum-rich alloys, Phys. Rev. B 64 (22) (2001) 224203, http://dx.doi.org/10.1103/PhysRevB.64.224203. <http://prb.aps.org/abstract/PRB/v64/i22/e224203>.

[23] Y. Qi, R.K. Mishra, Ab initio study of the effect of solute atoms on the stacking fault energy in aluminum, Phys. Rev. B 75 (22) (2007) 224105, http://dx.doi.org/10.1103/PhysRevB.75.224105. <http://link.aps.org/doi/10.1103/PhysRevB.75.224105>.

[24] J.P. Perdew, K. Burke, M. Ernzerhof, Generalized gradient approximation made simple, Phys. Rev. Lett. 77 (18) (1996) 3865–3868, http://dx.doi.org/10.1103/PhysRevLetter77.3865. <http://prl.aps.org/abstract/PRL/v77/i18/p3865_1>.

[25] P.E. Blöchl, Projector augmented-wave method, Phys. Rev. B 50 (24) (1994) 17953–17979, http://dx.doi.org/10.1103/PhysRevB.50.17953. <http://prb.aps.org/abstract/PRB/v50/i24/p17953_1>.

[26] G. Kresse, J. Furthmüller, Efficiency of ab-initio total energy calculations for metals and semiconductors using a plane-wave basis set, Comput. Mater. Sci. 6 (1) (1996) 15–50, http://dx.doi.org/10.1016/0927-0256(96)00008-0. <http://www.sciencedirect.com/science/article/B6TWM-3VRVTBF-3/2/88689b1eacfe2b5fe57f09d37eff3b74>.

[27] G. Kresse, D. Joubert, From ultrasoft pseudopotentials to the projector augmented-wave method, Phys. Rev. B 59 (3) (1999) 1758–1775, http://dx.doi.org/10.1103/PhysRevB.59.1758. <http://prb.aps.org/abstract/PRB/v59/i3/p1758_1>.

[28] H.J. Monkhorst, J.D. Pack, Special points for Brillouin-zone integrations, Phys. Rev. B 13 (12) (1976) 5188–5192, http://dx.doi.org/10.1103/PhysRevB.13.5188. <http://prb.aps.org/abstract/PRB/v13/i12/p5188_1>.

[29] M. Methfessel, A.T. Paxton, High-precision sampling for Brillouin-zone integration in metals, Phys. Rev. B 40 (6) (1989) 3616–3621, http://dx.doi.org/10.1103/PhysRevB.40.3616. <http://prb.aps.org/abstract/PRB/v40/i6/p3616_1>.

[30] F. Birch, The effect of pressure upon the elastic parameters of isotropic solids according to Murnaghan's theory of finite strain, J. Appl. Phys. 9 (4) (1938) 279–288, http://dx.doi.org/10.1063/1.1710417. <http://link.aip.org/link/?JAP/9/279/1>.

[31] F. Birch, Finite elastic strain of cubic crystals, Phys. Rev. 71 (11) (1947) 809–824, http://dx.doi.org/10.1103/PhysRev. 71.809. <http://prola.aps.org/abstract/PR/v71/i11/p809_1>.

[32] M.J. Besnus, A. Herr, A.J.P. Meyer, Magnetization of disordered cold-worked Fe–Al alloys up to 51 at.% Al, J. Phys. F: Metal Phys. 5 (11) (1975) 2138. <http://stacks.iop.org/0305-4608/5/i=11/a=026>.

[33] T. Uesugi, K. Higashi, First-principles studies on lattice constants and local lattice distortions in solid solution aluminum alloys, Comput. Mater. Sci. 67 (0) (2013) 1–10, http://dx.doi.org/10.1016/j.commatsci.2012.08.037. <http://www.sciencedirect.com/science/article/pii/S0927025612005290>.

[34] K.A. Gschneidner Jr., Physical properties and interrelationships of metallic and semimetallic elements, in: F. Seitz, D. Turnbull (Eds.), Solid State Physics: Advances in Research and Applications, vol. 16, Academic Press, 1964, pp. 275–426, http://dx.doi.org/10.1016/S0081-1947(08)60518-4. <http://www.sciencedirect.com/science/article/B8GXT-4SCVFB4-B/2/aef6f05362c12ca59b466bd2ece0d762>.

[35] J.C. Slater, Atomic radii in crystals, J. Chem. Phys. 41 (10) (1964) 3199–3204, http://dx.doi.org/10.1063/1.1725697. <http://dx.doi.org/doi/10.1063/1.1725697>.

[36] N. Kioussis, M. Herbranson, E. Collins, M.E. Eberhart, Topology of electronic charge density and energetics of planar faults in fcc metals, Phys. Rev. Lett. 88 (2002) 125501, http://dx.doi.org/10.1103/PhysRevLett.88.125501. <http://link.aps.org/doi/10.1103/PhysRevLett.88.125501>.

[37] S. Ogata, J. Li, S. Yip, Ideal pure shear strength of aluminum and copper, Science 298 (5594) (2002) 807–811, http://dx.doi.org/10.1126/science.1076652. <http://www.sciencemag.org/content/298/5594/807.abstract>.

[38] C. Brandl, P.M. Derlet, H.V. Swygenhoven, General-stacking-fault energies in highly strained metallic environments: ab initio calculations, Phys. Rev. B 76 (5) (2007) 054124, http://dx.doi.org/10.1103/PhysRevB.76.054124. <http://prb.aps.org/abstract/PRB/v76/i5/e054124>.

[39] C. Kittel, Free electron fermi gas, Introduction to Solid State Physics, eighth ed., Wiley, 2004. <http://www.amazon.com/Introduction-Solid-Physics-Charles-Kittel/dp/047141526X/ref=dp_ob_title_bk> (Chapter 6), p. 150.

[40] P.S. Branicio, J.Y. Zhang, D.J. Srolovitz, Effect of strain on the stacking fault energy of copper: a first-principles study, Phys. Rev. B 88 (2013) 064104, http://dx.doi.org/10.1103/PhysRevB.88.064104. <http://link.aps.org/doi/10.1103/PhysRevB.88.064104>.

[41] L. Romaner, C. Ambrosch-Draxl, R. Pippan, Effect of rhenium on the dislocation core structure in tungsten, Phys. Rev. Lett. 104 (2010) 195503, http://dx.doi.org/10.1103/PhysRevLett.104.195503. <http://link.aps.org/doi/10.1103/PhysRevLett.104.195503>.

[42] E. Pink, R.J. Arsenault, Low-temperature softening in body-centered cubic alloys, Progr. Mater. Sci. 24 (1980) 1–50, http://dx.doi.org/10.1016/0079-6425(79)90003-3. <http://www.sciencedirect.com/science/article/B6TX1-48JM55J-7/2/da32276dbf14ad725c474712b1a21794>.

[43] J. Eshelby, The continuum theory of lattice defects, in: F. Seitz, D. Turnbull (Eds.), Solid State Physics-Advances in Research and Applications, Solid State Physics, vol. 3, Academic Press, 1956, pp. 79–144, http://dx.doi.org/10.1016/S0081-1947(08)60132-0. <http://www.sciencedirect.com/science/article/B8GXT-4SC6VGJ-6/2/bc5d21481b1e1337a9bf8e669c81c6e6>.

[44] L. Deléhouzée, A. Deruyttere, The stacking fault density in solid solutions based on copper, silver, nickel, aluminium and lead, Acta Metallur. 15 (5) (1967) 727–734, http://dx.doi.org/10.1016/0001-6160(67)90353-7. <http://www.sciencedirect.com/science/article/pii/0001616067903537>.

[45] P.C.J. Gallagher, The influence of alloying, temperature, and related effects on the stacking fault energy, Metallur. Trans. 1 (9) (1970) 2429–2461, http://dx.doi.org/10.1007/BF03038370. <http://link.springer.com/article/10.1007/BF03038370>.

[46] J. Han, X. Su, Z.H. Jin, Y. Zhu, Basal-plane stacking-fault energies of Mg: a first-principles study of Li- and Al-alloying effects, Scr. Mater. 64 (8) (2011) 693–696, http://dx.doi.org/10.1016/j.scriptamat.2010.11.034. <http://www.sciencedirect.com/science/article/B6TY2-51J9DT4-1/2/7bd643980983ce6d6503954f42fa26a9>.

[47] M. Eberhart, The metallic bond: elastic properties, Acta Mater. 44 (6) (1996) 2495–2504, http://dx.doi.org/10.1016/1359-6454(95)00347-9. <http://www.sciencedirect.com/science/article/pii/1359645495003479>.

[48] Y. Aray, J. Rodriguez, D. Vega, Topology of the electron density and cohesive energy of the face-centered cubic transition metals, J. Phys. Chem. B 104 (19) (2000) 4608–4612, http://dx.doi.org/10.1021/jp993976a. <http://pubs.acs.org/doi/abs/10.1021/jp993976a>.

[49] H. Jones, The effect on lattice parameter and hardness of manganese in extended solid solution in aluminium, J. Mater. Sci. Lett. 1 (9) (1982) 405–406, http://dx.doi.org/10.1007/BF00724853. <http://dx.doi.org/10.1007/BF00724853>.

[50] D. Simonovic, M.H.F. Sluiter, Impurity diffusion activation energies in Al from first principles, Phys. Rev. B 79 (5) (2009) 054304, http://dx.doi.org/10.1103/PhysRevB.79.054304. <http://prb.aps.org/abstract/PRB/v79/i5/e054304>.

[51] U.F. Kocks, A.S. Argon, M.F. Ashby, Thermodynamic and kinetics of slip, Equilibrium, vol. 19, Pergamon Press Ltd, 1975, http://dx.doi.org/10.1016/0079-6425(75)90001-8. <http://www.sciencedirect.com/science/article/pii/0079642575900018> (Chapter 2), p. 27.

[52] D. Caillard, J. Martin, Thermally Activated Mechanisms in Crystal Plasticity, Pergamon Materials Series, vol. 8, Elsevier Science, 2003, http://dx.doi.org/10.1016/S1470-1804(03)80028-7. <http://www.sciencedirect.com/science/article/B8GWY-4NW5CT7-1/2/fe83871025b72ecb925ab27ef3424e86>.